Combining Plasma Extracellular Vesicle Let-7b-5p, miR-184 and Circulating miR-22-3p Levels for NSCLC Diagnosis and for Predicting Drug Resistance

G. P. Vadla[1], B. Daghat[1], A. Garcia[1*], G. Perez[1*], V. Ahmad[1], N. Patterson[1], Y. Manjunath[2], J.T. Kaifi[2,3], G. Li[2,3], and C.Y. Chabu[1,2,3‡]

1. Division of Biological Sciences, Columbia, MO, 65211.

2. Department of Surgery, School of Medicine, University of Missouri, Columbia, MO, 65212.

3. Siteman Cancer Center, Washington University, St. Louis, MO 63110.

[*] Equal contribution

[‡]Corresponding author: C.Y. Chabu (chabuc@missouri.edu)

Abstract

Low-dose computed tomography (LDCT) Non-Small Cell Lung (NSCLC) screening is associated with high false-positive rates, leading to unnecessary expensive and invasive follow ups. There is a need for minimally invasive approaches to improve the accuracy of NSCLC diagnosis. Plasma extracellular vesicle (EV) and circulating microRNA (miRNA) have been proposed as cancer screening biomarkers. However, the identification of highly sensitive and broadly predictive core miRNA signatures remains a challenge. Also, how these systemic and diverse miRNAs impact cancer drug response is not well understood. Using an integrative approach, we examined plasma EV and circulating miRNA isolated from NSCLC patients versus screening controls with a similar risk profile. We found that combining EV (Hsa-miR-184, Let-7b-5p) and circulating (Hsa-miR-22-3p) miRNAs abundance robustly discriminates between NSCLC patients and high-risk cancer-free controls. Diagnosed NSCLC patients harboring sensitizing mutations in epidermal growth factor receptor EGFR (T790M, L578R) are treated with Osimertinib, a potent tyrosine kinase inhibitor (TKI). Nearly all patients develop TKI resistance via complex mechanisms and progress. We found that Hsa-miR-22-3p, Hsa-miR-184, and Let-7b-5p functionally converge on WNT/βcatenin and mTOR/AKT signaling axes, known cancer therapy resistance signals. Targeting Hsa-miR-22-3p and Hsa-miR-184 desensitized EGFR-mutated (T790M, L578R) NSCLC cells to Osimertinib. These findings suggest that the expression levels of circulating hsa-miR-22-3p combined with EV hsa-miR-184 and Let-7b-5p levels potentially define a core biomarker signature for improving the accuracy of NSCLC diagnosis. Importantly, these biomarkers have the potential to enable prospective identification of patients who are at risk of responding poorly to Osimertinib alone but likely to benefit from Osimertinib/AKT blockade combination treatments.

Introduction

Lung cancer causes the most cancer-related deaths worldwide[1], with 85% of lung cancer patients present with non-small cell lung cancer (NSCLC) and 70% of the cases are diagnosed as late-stage disease[1-3]. The 5-year survival rate for late-stage NSCLC is 2-5% compared to 92% for early-stage disease[1], underscoring the importance of early detection.

Current lung cancer screening involves the use of the Lung imaging reporting and data system (Lung-RADS). This classification system relies on chest low-dose computed tomography (LDCT) scans: based on the numbers, size, appearance, and location of detected lung nodules, Lung-RADS assigns a score where Lung-RADS 1 means no lung nodules, Lung-RADS 2 and 3 represent probably benign lung nodules, whereas suspicious nodules with highest risk of cancer are categorized as Lung-RADS4) [4] However, LDCT has low specificity and a high false-positives rate (~23%)[5]. For patients who undergo multiple rounds of LDCT screening, the cumulative false-positive rate is estimated at 38-50% [5,6]. In addition to the unnecessary emotional distress, these over-diagnosed patients are subjected to costly and invasive follow ups before they are confirmed lung cancer free. There is a need for minimally invasive strategies that permit early and accurate detection of NSCLC.

Patients who are diagnosed with NSCLC are stratified to chemotherapy and/or immunotherapy, or targeted therapy based on the presence or absence of known NSCLC driver mutations in tissue biopsy analyses [7,8]. Depending on patients' ethnicity, activating mutations of epidermal growth factor receptor (EGFR) tyrosine kinase is found in 15-50% of NSCLC [9-11]. Patients harboring drug sensitizing EGFR mutations are treated with tyrosine kinase inhibitors or TKI. Some patients initially respond to tyrosine kinase inhibitors (TKI) but ultimately develop resistance: cancers acquire TKI-desensitizing EGFR mutations or activate compensatory signals,

70 including WNT/β-catenin, the mechanistic target of rapamycin mTOR, and AKT signaling to drive
71 cancer recurrence [12-20]. Screening for genetic alterations that activate these signaling pathways
72 provides a rationale for prioritizing treatment options that maximize the probability of achieving
73 durable outcomes. However, it is becoming increasingly evident that cancer cells develop drug
74 resistance via complex non-mutational mechanisms that involve emergent cell-cell interactions
75 mediated by microRNAs (miRNAs) [21-24]. miRNAs are short (19-23) non-coding nucleotides that
76 degrade protein transcripts and fundamentally impact signaling events [25-27]. These miRNAs are
77 released directly into the blood circulation (circulating miRNA) or secreted as extracellular
78 vesicles (EV) cargo to elicit signaling events in target cells [28,29]. The potential for EV miRNA as
79 minimally-invasive liquid biomarkers is now widely recognized [30,31].

80 In this study, we integrated EV and circulating blood miRNA analyses to identified EV
81 and miRNA combined features that robustly differentiate cancer patients from disease-free
82 controls. Further, the identified miRNAs converge on WNT/β-catenin and AKT/mTOR signaling
83 pathways, suggesting a role in drug-resistance and highlighting their potential as biomarkers for
84 predicting therapy response and for selecting patients that will likely benefit from AKT blockade.
85

86 **Results**

87 **CD9 and CD63, but not CD81, are enriched on NSCLC patients extracellular vesicles**

88 There is a critical need for sensitive, robust, and minimally-invasive tools for improving
89 the accuracy of NSCLC diagnosis. To this end, we interrogated plasma extracellular vesicles and
90 miRNA to identify molecular signatures that can discriminate between NSCLC patients and
91 healthy individuals with similar risk profiles. The US Preventive Services Task Force recommends
92 LDCT screening for at-risk individuals defined as 55-80 years of age with 30 or more pack-year

93 smoking history or have quit within the past 15 years [32]. Individuals ranging between 42 and 62
94 years of age with a qualifying smoking history were divided into two groups based on their initial
95 LDCT Lung-RADS scores 2 or 4 (Table 1, Lung-RADS2 screening controls versus Lung-RADS4,
96 *N*=20 per group).

97 We isolated plasma EV from all 40 individuals (Figure 1a) and performed nanoparticle
98 tracking analyses (NTA) to determine whether EV from Lung-RADS4 patients cohort exhibit
99 physical characteristics that are distinct from control cohort EV. Initial analyses revealed that EV
100 density was reduced in Lung-RADS4 patients compared to screening controls but these EV were
101 larger than Lung-RADS2 EV (Figure 1b, c).

102 LDCT has a false positive rate of 23-50% [5,6,33]. Consistent with this, follow up tissue
103 biopsies analyses revealed that 30% (6 out of 20) of the patients who were classified as Lung-
104 RADS4 at baseline LDCT screening did not have lung cancer (Table 1; group column, asterisk).
105 We asked whether the EV density and size characteristics can differentiate between true Lung-
106 RADS4 patients with lung cancer and the rest of the patients with benign lung nodules without
107 cancers (Lung-RADS2 plus the false-positive Lung-RADS4 patients). Although the trend of
108 reduced EV density and larger EV size in true Lung-RADS4 compared to controls persisted, these
109 differences were not statistically significant (data not shown).

110 We then asked whether EV membranes molecular profiles can differentiate between
111 screening controls, over-diagnosed individuals, and confirmed cancer patients. We first examined
112 the protein abundance of known EV membrane markers (the tetraspanins CD9, CD63, CD81, and
113 the resident EV protein flotillin). While EV isolated from all Lung-RADS4 (initial diagnosis,
114 including false-positive) patients and screening controls showed similar levels of CD81 and
115 flotillin, CD63 and, to a lesser extent, CD9 were specifically enriched in Lung-RADS4 EV (CD63

116 high, CD9 moderate) compared to Lung-RADS2 screening controls (CD63 low and CD9 low)
117 (Figure 1d). EV exclusively derived from confirmed NSCLC patients (IV^+) were CD63 high and
118 CD9 moderate) when compared to EV from false-positive patients (CD63 low and CD9 moderate)
119 or to screening controls (II: CD63 low and CD9 low) (Figure 1e-g). Consistent with these findings,
120 the ratio of CD9/CD63 levels distinguished confirmed cases from false-positive Lung-RADS4 or
121 screening individuals [Figure 1h, (mean±SD): 0.37±0.1 versus 1.86±0.66 versus 5.08±1.48,
122 respectively). Thus, EV CD9/CD63 expression ratio, but not EV physical characteristics, may help
123 differentiate NSCLC patients from cancer-free high-risk individuals.
124
125 **Plasma Let-7b-5p, miR-184, and miR-22-3p levels differentiate NSCLC patients from high-**
126 **risk individuals**
127 Next, we used next generation sequencing (NGS) approaches to profile EV miRNA from
128 Lung-RADS4 confirmed cancer patients or over-diagnosed Lung-RADS4 individuals or high-risk
129 screening controls (Lung-RADS2). We included circulating plasma miRNA because combining
130 multiple analytes from diverse biological sources have the potential to identify robust biomarkers.
131 We identified 58 differentially expressed miRNAs, including miRNA widely known to be
132 deregulated in cancers (Supplemental table 1). To identify a set of miRNAs that can robustly
133 discriminate between NSCLC and cancer-free individuals, we prioritized miRNAs that were
134 differentially expressed in at least two of the following comparisons: Lung-RADS2 versus Lung-
135 RADS4; Lung-RADS4 false positive versus confirmed cancer patients; Lung-RADS2 combined
136 with false-positive Lung-RADS4 patients versus confirmed cancer patients; any of the preceding
137 groups versus patients who rapidly progressed (LDCT imaging and/or death shortly after
138 sampling). We then focused on miRNAs showing significant performance (*P* and area under the

139 curve/AUC values) in receiver operating characteristic (ROC) analyses for further examination.
140 This approach led to the discovery of let-7b-5p, miR-184, and miR-22-3p as potential biomarkers
141 for discriminating cancer patients from high-risk controls.
142
143 Let-7b-5p levels were elevated in EV from Lung-RADS4 patients compared to EV from
144 screening patients alone (Figure 2a, e) or to screening patients plus false-positive Lung-RADS4
145 patients combined (Figure 2b, f). Also, miR-184 abundance was significantly reduced in Lung-
146 RADS4 EV compared to either control group (excluding or including false-positive Lung-RADS4
147 patients) (Figure 2c, d g, h). Circulating miRNA analyses showed that miR-22-3p levels were
148 reduced in Lung- RADS4 patients compared to either control group (Figure 2i, j, k, l). ROC curves
149 showed area under the curve (AUC) values above 70% and significant p-values for all of the
150 identified markers across comparisons (Figure 2e-h, 2k, l). The expression of these miRNAs was
151 independently verified in quantitative polymerase chain reaction (qPCR) experiments using EV or
152 plasma samples obtained from controls or false-positives or confirmed cancer patients (Figure 2n-
153 p and supplemental figure 1a-c). Further, the expression of Let-7b-5p, miR-184, miR-22-3p
154 showed no significant correlation with the gender, age, and pack-years smoking record of the
155 participants (supplemental figure 1d and supplemental table 1), providing additional statistical
156 rigor and indicating that the expression profile of these EV and circulating miRNAs is specifically
157 associated with disease status.
158 Furthermore, multiple logistic regression analyses of let-7b-5p, miR-184, and miR-22-3p
159 showed a combined ROC AUC value of 92.4% ($p<0.0001$, Figure 2m and supplemental table 2),
160 indicating remarkably high specificity and accuracy for these combined analytes to discriminate
161 between cancer patients and high-risk Lung-RADS2 controls. Thus, the abundance of EV let-7b-

162 5p, miR-184 combined with the levels of circulating miR-22-3p robustly discriminate between
163 lung cancer patients and high-risk individuals.
164
165 **Let-7b-5p, miR-184, and miR-22-3p converge on treatment-resistance mechanisms**
166 We considered the possibility that these EV and circulating plasma miRNAs (let-7b-5p,
167 miR-184, and miR-22-3p) mediate cell-cell communication events that support NSCLC disease
168 progression. First, we used the miRNA target proteins analysis platform MIRNET to identify
169 experimentally validated let-7b-5p, miR-184, and miR-22-3p target proteins. We prioritized
170 proteins that are targeted by at least two of the three miRNAs from experimental data (MIRNET
171 miR2gene)[34]. This approach identified 43 proteins (Figure 3a and supplemental table 3), which
172 were subsequently interrogated in Gene Ontology analyses using Kyoto Encyclopedia of Genes
173 and Genomes (KEGG) or Reactome classifications to derive signaling pathways. Cancer was the
174 most highly enriched KEGG term (Figure 3b, c), underscoring the robustness of our experimental
175 pipeline and the relevance of these miRNAs to cancer disease. Interestingly, KEGG and Reactome
176 signaling maps revealed that let-7b-5p, miR-184, and miR-22-3p converge on the activation of
177 WNT and PI3K-AKT-mTOR signaling (Figure 3c, d), suggesting that circulating and EV miRNAs
178 cooperatively regulate WNT and PI3K-AKT-mTOR activity in NSCLC. Activation of WNT or
179 PI3K-AKT-mTOR signaling in NSCLC tissues is associated with aggressive and therapy resistant
180 disease[35,36]. Considering that miR-184 and miR-22-3p are downregulated in cancer patients, this
181 suggests that plasma from high-risk yet cancer-free individuals contain EV and circulating
182 miRNAs that suppress WNT and the AKT signaling axis and that these mechanisms are restrained
183 in NSCLC patients.

184 Indeed, treatment of NSCLC cells (A549) with cancer patients EV elevated WNT and AKT
185 signaling levels compared to the effect of EV from screening controls, as determined by β-catenin
186 and phospho-AKT protein levels, respectively (Figure 3e, f).

187 Further, the uptake of EV by immune cells results in paracrine signaling loops that
188 ultimately accelerate disease progression via complex mechanisms[37-39]. We performed supernatant
189 transfer experiments and asked whether cancer patients EV activate AKT/mTOR in A549 cells
190 either directly or via immune cells. A549 cells were cultured in media conditioned by peripheral
191 blood mononuclear cells (PBMC) left untreated or treated with EV either from controls or from
192 cancer patients. Cancer patients EV/PBMC media dramatically stimulated phospho-AKT and
193 phospho-mTOR levels in A549 cells, compared to controls (Figure 3f, g). Note that EV from the
194 high-risk controls also stimulated mTOR signaling, possibly reflecting a NSCLC priming state
195 (see discussion). Consistent with this AKT/mTOR activating potential, EV/PBMC conditioned
196 media accelerated the growth of A549 cells (Figure 3h). Taken together, the above data argue that
197 plasma EV act directly or via immune cells to activate AKT in NSCLC.

198 Next, we sought to determine whether let-7b-5p, miR-184, and miR-22-3p mediate the
199 AKT activating effect of cancer EV and what implication this might have on NSCLC treatment
200 outcomes. Activating mutations in Epidermal Growth Factor Receptor (EGFR) signaling represent
201 one of the most known genetic alterations associated with NSCLC[40,41]. Patients harboring
202 sensitizing EGFR mutations (exon 19 deletion and L858R) respond favorably to first- and second-
203 generation Tyrosine Kinase Inhibitors/TKI (gefitinib, erlotinib, afatinib, and dacomitinib).
204 However, patients acquire TKI-desensitizing EGFR mutations (T790M) and become resistant to
205 these TKIs. Osimertinib, a third generation TKI selectively targets EGFR T790M and generates
206 significant clinical benefits in EGFR T790M patients [10,42-45]. Unfortunately, all patients ultimately

207 develop resistance to Osimertinib because they acquire an Osimertinib-desensitizing mutation
208 (C797S) or activate complex compensatory signals to resist drug-induced cell death and to promote
209 cancer cell proliferation [15,46-48]. Understanding the nature of these signals and how they are
210 activated have the potential to inform new treatment strategies for re-sensitizing patients to existing
211 TKIs.

212 We investigated a role for let-7b-5p, miR-184, and miR-22-3p in NSCLC response to
213 Osimertinib using H1975 NSCLC cells, which harbor L858R and T790M EGFR mutations. First,
214 H1975 cells were transfected with miR-184 and miR-22-3p inhibitors, mimicking their reduction
215 in cancer patient plasma and assessed the effect of miR-184/miR-22-3p inhibition on AKT activity.
216 The inhibitors reduced miR-184 and miR-22-3p levels in qPCR assays (Figure 3i and j,
217 respectively) and cooperatively elevated pAKT levels in H1975 cells (Figure 3k, l).

218 In reciprocal experiments we found that Lung-RADS2 EV, which overexpress miR-184
219 (Figure 2c, o), inhibit Osimertinib-induced AKT activity in H1975 cells (Figure 3l). Importantly,
220 inhibition of miR-22-3p in this setting was sufficient to dramatically unleash AKT (Figure 3l),
221 further highlighting the cooperation between these two miRNAs in modulating AKT activity.
222 Finally, we investigated the effect of miR-184/miR-22-3p inhibition on Osimertinib-induced cell
223 death. Consistent with AKT stimulation, miR-184/miR-22-3p inhibition significantly suppressed
224 Osimertinib-induced cell death (Figure 3m). Similar results were observed when miR-184/miR-
225 22-3p co-inhibited cells were treated in the presence of a let-7b-5p mimic (Figure 3m).

226 AKT activation is associated with NSCLC resistance to TKI, leading to reduced patient
227 survival time [35,36]. Thus, we sought to determine to what extent reduced miR-184/miR-22-3p tumor
228 expression correlates with reduced patient survival using the cancer genome atlas (TCGA) LUAD
229 patient tumor miRNA expression and survival data. We did not detect any significant survival

230 difference between patients whose tumors express low miR-22-3p (Figure 3n). However, patients
231 with low miR-184 tumor expression had a significantly shorter survival time compared to patients
232 with higher miR-184 tumor expression (Figure 3o, Hazard Ratio 2.09, 95% CI: 1.13, 3.84,
233 $p<0.018$). Interestingly, patients with miR-184/miR-22-3p co-repressed tumors experienced even
234 shorter survival time compared to patients with high miR-184/miR-22-3p tumor expression
235 (Figure 3p, Hazard Ratio 3.43, 95% CI: 1.26, 9.32, $p< 0.016$). Note that the survivorship of miR-
236 184/miR-22-3p tumor low patients is significantly lower than that of patients with tumor low miR-
237 184 alone or miR-22-3p alone. This is consistent with AKT activation in miR-184/miR-22-3p co-
238 inhibited NSCLC patients' plasma and treatment resistance.
239 Thus, EV (let-7b-5p, miR-184) and circulating (miR-22-3p) plasma miRNA likely modulate
240 NSCLC response to Osimertinib, highlighting a novel mechanism of resistance and suggesting
241 that these biomarkers may assist in the selection of patients that will likely benefit from
242 Osimertinib/AKT blockade combination treatments.
243
244 **Discussion**
245 The implementation of LDCT in NSCLC screening has reduced patient deaths by ~20% [5].
246 However, LDCT screening has a 23-50% false-positive rate [5,6,33], causing unnecessary exposure
247 to radiation, costly and invasive follow-up studies for these mis-diagnosed patients. Additional
248 strategies are needed to improve NSCLC screening accuracy.
249 Here we report the identification of a set of miRNAs (let-7-5p, miR-184 from EV and miR-
250 22-3p from circulating miRNAs) that distinguishes NSCLC patients from high-risk controls. In
251 addition, we found that the EV markers CD9, CD63, but not CD81 or flotillin, are differentially
252 expressed in NSCLC patients compared to high-risk controls.

253 Some of the unique features of this study include the fact that reference and disease cohorts
254 were controlled for risk profiles, reducing noise and elevating the relevance of the identified
255 biomarkers in NSCLC. Also, circulating miRNA are gaining much interest as potential biomarkers
256 in lung cancer [30,31]. Different from others, our study integrates plasma and EV miRNAs to not only
257 identify potential core molecular signatures for NSCLC risk management but to also highlight a
258 plausible cooperation between these miRNAs in influencing patients' drug response. Combining
259 multiple analytes of diverse biological origins (EV surface markers, EV and plasma miRNAs) also
260 maximizes robustness in diagnostics. Consistent with this, our biomarkers were able to
261 differentiate confirmed NSCLC patients from LDCT false-positives, suggesting that addition of
262 these non-invasive biomarkers to LDCT screening has the potential to improve diagnosis accuracy.
263 Confirmed NSCLC patients are stratified to diverse treatment options, including
264 chemotherapy, immunotherapy, and targeted therapies based on histological and genetic mutations
265 profiles obtained from tissue biopsies. Due to positional constraints, however, tissues biopsies
266 often fail to capture the broader complexity of genetic driver mutations, leading to incomplete
267 targeted therapy responses. The profiling of cancer-derived EV from patients' plasma may provide
268 deeper insights into the overall cancer mutational landscape of the tumor and thus better guide
269 treatment decisions in the future. Indeed, pathway analyses of let-7b-5p, miR-184, and miR-22-3p
270 target proteins revealed that these miRNAs converge on therapy resistance signals, including AKT.
271 We propose that circulating and EV miRNAs functionally cooperate to modulate oncogenesis or
272 patients' clinical outcomes (Figure 3q, r). The AKT-suppressing miRNAs miR-184/miR-22-3p
273 function as tumor suppressors and delay oncogenesis (Figure 3q). Cancers downregulate the
274 expression of these miRNAs and/or reduce their systemic abundance via an unknown mechanism,
275 leading to high baseline AKT activity and potentially resulting into accelerated cancer growth and

276 drug resistance (Figure 3r). EV and plasma miRNAs may act directly or via tumor-interacting
277 immune components to modulate tumor cell signaling and behavior. Mimicking the expression
278 profile of miR-184 (EV) and miR-22-3p (plasma) in NSCLC patients' blood using miRNA
279 inhibitors cooperatively activated AKT and desensitized NSCLC cells (H1975) to Osimertinib.
280 Thus, Let-7b-5p, miR-184, and miR-22-3p represent liquid biopsy biomarkers that will potentially
281 assist with the identification of patients that will likely benefit from Osimertinib/AKT blockade
282 combination treatments. AKT inhibition re-sensitizes TKI-resistant NSCLC cells to erlotinib and
283 gefitinib[49]. A clinical trial evaluating the efficacy of combining Osimertinib with aspirin (an AKT
284 inhibitor) in advanced NSCLC patients is pending (NCT04184921). Further, aberrant activation
285 of AKT/mTOR and WNT/β-catenin signaling are associated with therapy resistance across
286 different cancer types, suggesting broad translatability for these markers and their underlying
287 mechanisms of action. Future studies will include determining to what extent blood levels of Let-
288 7b-5p, miR-184, and miR-22-3p predict disease relapse in larger patient cohorts.

289 We noted that EV derived from high-risk control patients triggered mTOR activation in
290 A549 cells. We cannot rule out the possibility that this EV-induced mTOR activation is specific
291 to A549 cells, but it is likely that this effect reflects a priming state that precedes NSCLC onset in
292 these high-risk patients.

293 Finally, the observation that circulating and EV miRNAs that suppress cancer cell survival
294 and growth signals are upregulated in blood from high-risk cancer-free individuals compared to
295 cancer patients also provides insights into why, despite having comparable NSCLC risk profiles,
296 some individuals do not develop cancer, but others do.

297

298 **Ethical considerations**

299 All blood samples were collected with participants' written informed consent and in compliance
300 with the University of Missouri ethical guidelines. The protocol was approved by the University
301 of Missouri Ethics committee (IRB approval #2010166).
302
303 **Materials and methods**
304 **Isolation of extracellular vesicles and circulating micro-RNA**
305 Patients' blood was double-centrifuged to remove platelets and the platelet-poor plasma was used
306 for EV analysis. Purification of the EVs was done through size exclusion chromatography (SEC)
307 using qEV70s single columns (ddIzon, Netherlands). These columns were filled with 150 µl of
308 plasma and used based on recommendations from the manufacturer; fraction 8 through 11 were
309 collected and pooled to obtain the fraction of purified EVs. The particle size and concentration for
310 all EV samples were determined using nanoparticle tracking analysis (NTA).
311 Total RNA extraction was performed as previously described [50] using 200 µl of plasma or 200 µl
312 of pooled EV fractions and the miRNeasy mini kit (Qiagen). Samples were thawed at room
313 temperature followed by centrifugation at 12,000×g for 5 minutes at 4°C to remove any debris.
314 Extraction was conducted by use of the miRNA easy Qiagen kit. For homogenization, 200 µL of
315 plasma/EV suspension were mixed with 1000 µL Qiazol and 1 µL of a mix of 3 synthetic spike-
316 in controls (Qiagen, Germany). After a 10-minute incubation at room temperature, 200 µL
317 chloroform were added to the lysates followed by cooled centrifugation at 12,000×g for 15 minutes
318 at 4°C. Precisely 650 µL of the upper aqueous phase were mixed with 7 µL glycogen (50 mg/mL)
319 to enhance precipitation. Samples were transferred to a miRNeasy mini column, and RNA was
320 precipitated with 750 µL ethanol followed by automated washing with RPE and RWT buffer in a

321 QiaCube liquid handling robot. Finally, total RNA was eluted in 30 µL nuclease free water and
322 stored at -80°C until further use.
323
324 **Electron microscopy**
325 Exosomes were processed for negative staining as described in M. Rames, et al. [51]. Briefly, 5 µL
326 of purified EV sample was applied to a freshly glow discharged (Pelco Easiglow, Ted Pella
327 Redding CA) carbon coated TEM grid (Electron Microscopy Sciences, Hatfield PA) over
328 ice. Samples were washed three times with distilled water, incubated 2 min on 2%
329 paraformaldehyde (Electron Microscopy Sciences), then incubated for 30 sec on 2% uranyl acetate
330 (aqueous, Electron Microscopy Sciences) and back-blotted with filter paper (Whatman P1, Fisher
331 Scientific) and allowed to dry. Images were collected on a JEOL JEM 1400 transmission electron
332 microscope operated at 120V equipped with a Gatan Ultrascan 1000 CCD camera.
333
334 **Small RNA sequencing**
335 Small RNA sequencing was performed as described previously [52]. Equal volumes of total RNA (2
336 µL) were used for small RNA library preparation using the Clean Tag small RNA library
337 preparation kit (TriLink Biotechnologies, US). that utilizes chemically modified adapters to
338 prevent formation of adapter dimers [53]. Adapter-ligated libraries were amplified using barcoded
339 Illumina reverse primers in combination with the Illumina forward primer. A pool consisting of
340 40 plasma samples, and a second pool consisting of 40 EV samples was prepared by mixing
341 samples at equimolar rates based on a DNA-1000 bioanalyzer results (Agilent, CA). The DNA
342 library pool underwent size-selection (BluePippin, SageScience, US) to enrich for microRNAs
343 with an insert size of 18-36 nt, corresponding to a library size of approximately 145 bp.

344 Sequencing was performed on an Illumina NextSeq 550 with 75 bp single end runs. Overall quality
345 of the next-generation sequencing data was evaluated automatically and manually with FastQC
346 v0.11.8 and MultiQC v1.7. Reads from all passing samples were adapter trimmed and quality
347 filtered using Cutadapt v2.3 and filtered for a minimum length of 17nt. Mapping steps were
348 performed with bowtie v1.2.2 and miRDeep2 v2.0.1.2, whereas reads were mapped first against
349 the genomic reference GRCh38.p12 provided by Ensemble allowing for two mismatches and
350 subsequently miRBase v22.1, filtered for miRNAs of hsa only, allowing for one mismatch. For a
351 general RNA composition overview, non-miRNA mapped reads were mapped against RNAcentral
352 and then assigned to various RNA species of interest.
353 Statistical analysis of preprocessed NGS data was done with R v3.6 and the packages pheatmap
354 v1.0.12, pcaMethods v1.78 and genefilter v1.68. Differential expression analysis with edgeR v3.28
355 used the quasi-likelihood negative binomial generalized log-linear model (GLM) functions
356 provided by the package. False discovery rate (FDR) correction was performed to adjust for
357 multiple testing, and a cut-off of FDR < 5% was applied.
358
359 **Target network analysis**
360 miRNA target network analyses and genes ontology enrichments analyses (KEGG and Reactome)
361 were conducted using miRNet (www.mirnet.ca).
362
363 **Cell lines and cell culture**
364 The human lung cancer cell line A549 were grown in Dulbecco's Modified Eagle Medium
365 (DMEM, 11965-092), with L-Glutamine, and high glucose supplemented with 10% FBS. Cells
366 were grown in the nutrient medium as suggested by ATCC. Cells were incubated in a humidified

367 incubator with 5% CO2 at 37°C. H1975 cells were grown in ATCC-formulated RPMI-1640
368 Medium (ATCC, Cat number 30-2001), with 10% FBS (fetal bovine serum) at 37 C, 5% CO2.
369

370 **Peripheral blood mononuclear cells (PBMC) isolation**

371 10 mL of blood from healthy individual was collected into EDTA coated anti-coagulant vacutainer
372 tubes (Cat #367899, BD Biosciences). Transferred onto 50 mL sterile 50 mL centrifuge tube and
373 added equal volume with of ice cold DPBS pH 7.4 and gently mix by inversion. Using transfer
374 pipette, carefully transferred diluted blood to sterile centrifuge tube containing 10 mL of Ficoll-
375 Paque plus (Amersham #17144003,) then centrifuge at 2000 rpm for 25 min. after centrifuged
376 from the fractionated phases, carefully collect the PBMCs fraction between ficol-paque and plasma
377 layer. Collected PBMCs washed with ice cold PBS and centrifuge at 1700 rpm for 10 min. pellet
378 re-suspended with 2 ml of Pharm Lyse lysing buffer (Biosciences #555899), mix well incubate at
379 37°C for 4 min and adjust volume with PBS to 50 mL and proceed with centrifuge at 1700 rpm for
380 10 min. PBMC pellet re suspend in PBS with 1×10^{6} cells/mL for further experimental purpose.
381

382 **EV/PBMC supernatant transfer experiments**
383
384 Isolated human PBMCs were seeded and grown in 6 well culture dish with hybridoma-(SFM)
385 serum free medium (Cat #12045076, Gibco). PBMCs were treated with patient EVs under serum
386 free conditions for 24 hrs. After incubation cell free PBMC or EV/PBMC conditioned media were
387 collected and used for culturing A549 cells. After 24 hours A549 cells were collected for cell
388 counting or lysed for Western blotting.
389

390 **Western blotting**
391

392 *Extracellular vesicles (EV)*. EV pellets were dissolved in 100 ul of modified lysis buffer (20 mM
393 Tris-HCl pH-7.5, 150 mM NaCl, 1mM Na_2EDTA, 1mM EGTA, 1%TritonX-100, 2.5 mM sodium
394 pyrophosphate, 1 mM b-glycerophosphate, 1 mM Na_3VO_4, 1μg/mL leupeptin). Samples were
395 treated with 10% glycerol, 1 M urea, 0.1% SDS, and loading buffer before SDS-PAGE. Gels were
396 transferred onto PVDF membranes and stained with primary antibodies against CD-9 (1:1000,
397 Millipore #CBL162,), CD-63 (1:1000, Molecular probes #A15712), CD-81 (1:1000, BioLegend
398 #349561), and flotillin (1:1000, Santa Cruz #74566). Secondary antibodies were anti-mouse
399 horseradish peroxidase (1:10000, Invitrogen #31430). Protein bands were detected using the Pierce
400 ECL Chemiluminescence kit western (Thermo Fisher #32106) and the ChemiDoc™ Imaging
401 System, Bio-Rad Laboratories Inc.
402 *EV-treated A549 cells*. A549 cells were cultured with similar loads of EV derived either from high-
403 risk controls or confirmed lung cancer patients. Lysates were prepared in lysis buffer (20 mM Tris-
404 HCl pH-7.5, 150 mM NaCl, 1 mM Na_2 EDTA, 1 mM EGTA, 1%TritonX-100) and processed for
405 Western blotting. Blots were stained against β-catenin to determine WNT signaling levels and
406 GAPDH as a loading control (1:1000, Cell signaling #5174S). Secondary horseradish peroxidase
407 (HRP) antibodies were obtained from Invitrogen. Pierce ECL Chemiluminescence kit (Thermo
408 Fisher scientific #32106) and the ChemiDoc Imaging System (Bio-Rad) were used to detect
409 protein bands.
410 A549 cells were washed with PBS and lysed in a lysis buffer (20 mM Tris-HCl pH-7.5, 150 mM,
411 NaCl, 1 mM Na_2EDTA, 1 mM EGTA, 1%Triton, 2.5 mM sodium pyrophosphate, 1 mM b-
412 glycerophosphate, 1 mM Na3VO4, 1μg/ml leupeptin) supplemented with protease and a
413 phosphatase inhibitor cocktail (Cell Signaling #9803S). Proteins were electrophoresed on SDS-
414 PAGE using 4-20% Mini-PROTEAN® TGX™ precast gel (Biorad #456-1094,), transferred onto

415 methanol pretreated PVDF membrane. PVDF membranes were probed overnight with mouse anti
416 β-catenin (DSHB, #PY489), mouse anti-mTOR (1:1000, Santa Cruz, #517464) and mouse anti-
417 GAPDH (DSHB, #2G7) at 4°C and after washing 3 times, membranes were incubated with anti-
418 rabbit mouse horseradish peroxidase (HRP) (1:5000, #31460, Invitrogen). Primary or secondary
419 antibodies were diluted in 5% BSA-TBST. Anti-mouse horseradish peroxidase (HRP) (1:5000,
420 Invitrogen #31430,), anti-rabbit horseradish peroxidase (HRP) (1:5000, Invitrogen #31460,) used
421 to develop respective blots. Membranes were developed using Pierce ECL western blotting
422 substrate (Thermo Fisher scientific #32106,) and imaged on ChemiDoc™ MP Imaging System,
423 Bio-Rad Laboratories Inc.
424 *H1975 cells*. H1975 cells were lysed in 1× RIPA buffer (Thermofisher #89900) containing 1×
425 Halt™ Protease Inhibitor Cocktail (Thermofisher #78425). Proteins were separated on a 4-12%
426 Bis-Tris gel (Invitrogen, Cat# NP0321) and transferred to PVDF membranes. Membranes were
427 incubated with primary antibodies against Phospho-AKT (1:5000, Proteintech #66444-1-Ig,) or
428 GAPDH (Sigma #G8795) overnight at 4ºC. Secondary antibodies were purchased from Cell
429 Signaling (Cat#7076). Blots were developed with Immobilon Western Chemiluminescence Kit
430 (Millipore, #WBKLS0500).
431 miRNA Transfections and Osimertinib treatments miRNA stock was prepared by suspending in RNAse-
432 free water. Cells were seeded such that they were 70-80% confluent at the time of transfection. Cells were
433 allowed to adhere for 24 hrs and then transfected with 25 nM of miRNA inhibitors against hsa-miR184
434 (Sigma #HSTUD0282), hsa-miR22-3p (Sigma #HSTUD0393) or 100 nM of hsa-let7b-5p miRNA mimic
435 (Sigma #HMI0007) using Lipofectamine 3000 (Invitrogen #L3000001). Osimertinib (100 nM) was added
436 an hour after transfection to cells. Cells were allowed to incubate with transfection mix for 24 hrs at 37
437 ºC, 5% CO_2 and then washed with 1× PBS and trypsinized to be used for cell count and Western blotting.

438

439 **cDNA synthesis and qRT-PCR**

440 cDNA synthesis was carried out using the miRCURY LNA RT Kit (Qiagen #339340) from human
441 purified EVs or plasma RNA (10 ng) according to manufacturer's instructions. The synthesized
442 CDNA diluted in nuclease free water and stored until further use at -80°C as per the kit instructions.
443 Quantitative polymerase chain reaction was conducted using miRCURY LNA miRNA SYBR
444 PCR kit (Qiagen #339345) as per manufacturer's instruction on BioRad CFX96^{TM} System in 96-
445 well plates in 3-6 repeats. A two-step thermal cycling protocol i.e., 95°C for 2 min followed by 40
446 cycles at 95°C for 10 sec and 56°C for 60 sec, was used. A no-reverse transcriptase (NRT) and no-
447 template control (NTC) were included in each reaction to check for primer specificity and any
448 non-specific amplification. miRNA targets include miRNA-184 (Qiagen #YP00204601), miRNA-
449 21-5p (Qiagen #YP00204230), Let-7b-5p (Qiagen #YP00204750), miRNA 22-3p (Qiagen
450 #YP00204606). The expression levels of each miRNA target were normalized to calibrators U6-
451 snRNA or GAPDH. Fold changed of miRNA was calculated by ΔΔCt and $2^{-\Delta\Delta Ct}$ method. ΔCt was
452 calculated by subtracting the average of Ct values of calibrator from Ct values of target miRNA.
453 ΔΔCt was computed by subtracting ΔCt of the screening control from ΔCt of RADS IV group.

454 **Patient Data Analysis**

455 MicroRNA expression (miRNAseq) and clinical data from Lung adenocarcinoma (LUAD) were
456 collected from the publicly accessible TCGA database using the Bioconductor tool TCGA
457 Biolinks RTCGA R packages. The "surv_cutpoint" function of the "survminer " R package was
458 used to identify high versus low expressing patients' samples for survival analysis. Survminer uses
459 selected rank statistics to determine the optimal cut-point of a continuous variable in an unbiased

460 manner. Kaplan–Meier (KM) survival plots and related statistics were generated using the Survival
461 R package. (Supplemental information 2)
462
463 **Authors contributions**
464 C.Y.C conceived the study. A.G and C.Y.C wrote the manuscript. J.K was the IRB primary
465 investigator and coordinated the acquisition of patient blood samples with Y.M. A.G and G.P
466 performed miRNA and miRNA target analyses. G.P.V and Y.M processed patient blood samples.
467 V.A isolated patients EV and performed qPCR analyses. G.P.V carried out qPCR analyses,
468 biochemical and morphometric EV studies. B.D planned and performed all cell growth and cell
469 death and Western blotting analyses. N.P performed TCGA miRNA expression patient survival
470 analyses. C.Y.C and G.L examined the data. This work was funded by MU start-up funds to C.Y.C,
471 MOLSAMP support to A.G, and NIH-IMSD support to G.P.
472
473 **Acknowledgment**
474 We thank D. Porcini and R. Kannan for providing H1975 cells, E. King for assistance with
475 developing the R code for TCGA studies. We also thank M. Hackl and A. Diendorfer (TAmiRNA,
476 Austria) for assistance with NGS analyses.
477 **Competing Interests**
478 Parts of the presented data are under consideration for patent filing (C.Y.C). All other authors
479 declare no conflicts.
480
481 **Figure Legends**
482 **Table 1. Participants profile**

483 Table showing each patient's description including, age, gender, smoking history, and cancer
484 progression status. False positive diagnoses are denoted with an asterisk (*) in the Group column.
485 Group A and B contain individuals with lung-RADS2 or lung-RADS4 initial LDCT findings,
486 respectively.
487
488 **Figure 1. CD9 and CD63, but not CD81, are enriched on NSCLC EV**
489 a) Representative transmission electron micrograph of the isolated extracellular vesicles (EV).
490 b and c) Nanoparticle tracking analyses (NTA) data showing EV concentrations (particles/mL) (b)
491 and size distribution (c). One-way ANOVA analysis was performed to determine statistical
492 significance, *<0.05.
493 d) Western blot image showing abundance of EV markers (CD81, CD63, CD9, and Flotillin) in
494 EV isolated from blood samples obtained from screening controls (LNG-RADS II) or LNG-RADS
495 IV individuals.
496 e) Western blot images from triplicate samples showing CD9 and CD63 protein levels in EV
497 extracted from LNG RADS II or confirmed cancer patients (IV^+) plasma or disease-free LNG-
498 RADS IV (IV^-) individuals. Flotillin protein levels are used as loading controls. These experiments
499 are shown in triplicates. (f, g) Relative quantification of CD9 and CD63 protein levels in Western
500 blot shown in (e). Proteins levels are denoted as ratio of pixel intensities mean values quantified
501 from each of the three replicates and normalized to Flotillin. (h) Ratio of CD9:CD63 protein band
502 intensities presented in (e). Quantification of band intensities (pixels) was performed using ImageJ.
503 Bars represent data as mean ± SD. P-values are derived from t-test. *p<0.05, **p<0.01,
504 ***p<0.001.
505

506 **Figure 2. Identification of unique EV and circulating miRNA profiles Lung-RADS4 cancer**
507 **patients**

508 a-l) Next Generation Sequencing (NGS) of blood EV or circulating miRNA identified Let-7b-5p,
509 miR-184, and miR-22-3p as differentially expressed in NSCLC patients compared to controls. Let-
510 7b-5p (a, b) and mir-184 (c, d) are deregulated in EV and mir-22-3p in plasma (i, j). The relative
511 abundance of the indicated miRNA in screening controls (blue) versus confirmed diseased patients
512 only (green) or versus all lung-RADS2 plus false-positive lung-RADS4 (magenta) are shown in
513 (a-d) and (I, j), respectively. P-values were Benjamini-Hochberg adjusted. *p<0.1, **p<0.05,
514 ***p<0.01,****p<0.001. Note that 2-3 patient samples with undetectably low reads were excluded
515 from the analysis. Corresponding Reads per million (RPM) were used to plot miRNA levels in
516 confirmed cancer patients versus disease-free individuals and to perform ROC analysis shown in
517 (e-h, k, l). EdgeR generalized linear models (GLM) were used to assess significance of miRNA
518 regulations.

519 Multiple logistic regression analysis was performed to determine the combined classification
520 performance of the three miRNA biomarker candidates (m). Statistical significance of miRNA
521 regulations was determined by EdgeR GLM, as indicated above.

522 (n-p) Quantitative Polymerase Chain Reaction (qPCR) data showing expression fold changes
523 (means) of let-7b-5p (n) or miRNA-184 (o) or miRNA-21-5p (n) or miRNA-22-3p (p) in EV
524 samples obtained from confirmed cancer patients (IV+) versus screening controls (II). RNA
525 samples were pooled from 14 cancer patients and 14 randomly selected screening individuals.
526 Expression was normalized to *GAPDH*. Error bars denote SD values. *P* values are derived from
527 student t-test analyses.

528

529 **Figure 3. Let-7b-5p, miR-184, and miR-22-3p converge on AKT/mTOR and WNT/β- catenin**
530 **therapy resistance pathways**.
531 a) Venn diagram showing the number unique of shared protein targets between the selected
532 miRNAs.
533 b) MIRNET star-network showing proteins that are targeted by at least two of the three miRNAs
534 (blue squares).
535 c, d) KEGG (c) or Reactome (d) classification analyses of the identified proteins show a
536 convergence onto PI3K-AKT-mTOR (c, magenta label and d, green label) and WNT/β-catenin (d,
537 brown label) signaling pathways. The underlying target genes are shown in corresponding color
538 in "b".
539
540 e) Western blot image from A549 cells treated with equal quantity of EV from cancer patients or
541 from high-risk screening controls. Blots were stained against β-catenin to detect WNT signaling
542 levels or GAPDH as a loading control.
543 f, g) Western blot images from A549 cells cultured in standard media or media conditioned with
544 PBMC in the absence or presence of patients EV (f, lanes1-4). Also, A549 cells were treated
545 directly with cancer patients or control EV (f, lanes 5 and 6). Blots were stained against phospho-
546 AKT1 (f) or phospho-mTOR(g) or GAPDH as a loading control (f, g). A549 cell numbers from
547 supernatant transfer experiments (f, lanes 1-4) are shown in "h" as average cell numbers from
548 triplicate experiments. Error bars denote SD values. *P* values are derived from student t-test
549 analyses.

550 i, j) qPCR data showing mean expression fold changes of miR-184 (i) or miR-22-3p (j) in H1975
551 cells transfected with miR-184 (i) or miR-22-3p inhibitors (j) (blue bars) compared to untreated
552 H1975 control cells (red bars). Expression was normalized to *GAPDH.*
553 k) Western blot images from H1975 cells left untreated or treated with miR-22-3p or miR-184
554 inhibitors and blotted against phospho-AKT1 or GAPDH (loading control).
555 l) Image of a Western blot from untreated H1975 cells or H1975 cells treated with equal portions
556 of EV from screening controls (RADS-II) or with inhibitors against miR-22-3p and/or miR-184
557 inhibitors followed with Osimertinib (100nM) treatments. Western blots were stained against
558 phospho-AKT or GAPDH (loading control).
559 m) Graph showing the proportion of H1975 cell death across the indicated conditions using Trypan
560 blue exclusion assays. These cell death assays were performed in triplicates and the results are
561 shown as the average proportion (percentage) of dead cell across replicates for each treatment
562 conditions. Error bars denote standard deviations and p-values were derived from t-tests.
563
564 n-p) Survivorship comparison data using miR-184 and/or miR-22-3p expression data in TCGA-
565 LUAD and the Bioconductor tool TCGA Biolinks RTCGA R packages. The "surv_cutpoint"
566 function of the “survminer ” R package was used to identify high versus low expressing patients’
567 samples for miR-22-3p (n) or miR-184 (o) or both (p) in Cox regression analyses. Survminer uses
568 selected rank statistics to determine the optimal cut-point of a continuous variable in an unbiased
569 manner. The related bioinformatics and statistics are presented in supplementary information 1.
570 q, r) proposed model summarizing the role of mir-184/mir-22 in Osimertinib drug response. EV
571 (mir-184) and circulating (mir-22) plasma miRNAs cooperatively target and modulate AKT
572 activity. (q) Cancer-free high-risk individuals up-regulate EV mir-184 and circulating mir-22,

573 keeping AKT levels generally low. In the context of genetic driver mutations, this low AKT
574 activity delays oncogenesis. Similarly, cancer patients with high EV mir-184 and circulating mir-
575 22-3p maintain AKT below an activity threshold required for AKT-mediated drug resistance,
576 leading to positive drug response. However, AKT baseline activity is elevated in patients with low
577 mir-184/mir-22 levels such that even a modest stimulation of AKT drives AKT above the drug-
578 resistance activity threshold, leading to relapses and poor clinical response (r).
579

580 **Data availability**

581 All data will be made available upon reasonable request.

582 **Reference**
583

584 1 Molina, J. R., Yang, P., Cassivi, S. D., Schild, S. E. & Adjei, A. A. Non-small cell lung cancer:
585 epidemiology, risk factors, treatment, and survivorship. *Mayo Clin Proc* **83**, 584-594,
586 doi:10.4065/83.5.584 (2008).
587 2 Lemjabbar-Alaoui, H., Hassan, O. U., Yang, Y. W. & Buchanan, P. Lung cancer: Biology and
588 treatment options. *Biochim Biophys Acta* **1856**, 189-210, doi:10.1016/j.bbcan.2015.08.002
589 (2015).
590 3 Travis, W. D. *et al.* The 2015 World Health Organization Classification of Lung Tumors: Impact of
591 Genetic, Clinical and Radiologic Advances Since the 2004 Classification. *J Thorac Oncol* **10**, 1243-
592 1260, doi:10.1097/JTO.0000000000000630 (2015).
593 4 Pinsky, P. F. *et al.* Performance of Lung-RADS in the National Lung Screening Trial: a retrospective
594 assessment. *Ann Intern Med* **162**, 485-491, doi:10.7326/M14-2086 (2015).
595 5 National Lung Screening Trial Research, T. *et al.* Reduced lung-cancer mortality with low-dose
596 computed tomographic screening. *N Engl J Med* **365**, 395-409, doi:10.1056/NEJMoa1102873
597 (2011).
598 6 Lopes Pegna, A. *et al.* Four-year results of low-dose CT screening and nodule management in the
599 ITALUNG trial. *J Thorac Oncol* **8**, 866-875, doi:10.1097/JTO.0b013e31828f68d6 (2013).
600 7 Haslam, A. & Prasad, V. Estimation of the Percentage of US Patients With Cancer Who Are Eligible
601 for and Respond to Checkpoint Inhibitor Immunotherapy Drugs. *JAMA Netw Open* **2**, e192535,
602 doi:10.1001/jamanetworkopen.2019.2535 (2019).
603 8 Hirsch, F. R. *et al.* Lung cancer: current therapies and new targeted treatments. *Lancet* **389**, 299-
604 311, doi:10.1016/S0140-6736(16)30958-8 (2017).
605 9 Chen, Y. M. Update of epidermal growth factor receptor-tyrosine kinase inhibitors in non-small-
606 cell lung cancer. *J Chin Med Assoc* **76**, 249-257, doi:10.1016/j.jcma.2013.01.010 (2013).
607 10 Mok, T. S. *et al.* Gefitinib or carboplatin-paclitaxel in pulmonary adenocarcinoma. *N Engl J Med*
608 **361**, 947-957, doi:10.1056/NEJMoa0810699 (2009).
609 11 Zhou, C. *et al.* Erlotinib versus chemotherapy as first-line treatment for patients with advanced
610 EGFR mutation-positive non-small-cell lung cancer (OPTIMAL, CTONG-0802): a multicentre, open-
611 label, randomised, phase 3 study. *Lancet Oncol* **12**, 735-742, doi:10.1016/S1470-2045(11)70184-
612 X (2011).
613 12 Arcila, M. E. *et al.* Rebiopsy of lung cancer patients with acquired resistance to EGFR inhibitors
614 and enhanced detection of the T790M mutation using a locked nucleic acid-based assay. *Clin*
615 *Cancer Res* **17**, 1169-1180, doi:10.1158/1078-0432.CCR-10-2277 (2011).
616 13 Yu, H. A. *et al.* Analysis of tumor specimens at the time of acquired resistance to EGFR-TKI therapy
617 in 155 patients with EGFR-mutant lung cancers. *Clin Cancer Res* **19**, 2240-2247, doi:10.1158/1078-
618 0432.CCR-12-2246 (2013).
619 14 Sequist, L. V. *et al.* Genotypic and histological evolution of lung cancers acquiring resistance to
620 EGFR inhibitors. *Sci Transl Med* **3**, 75ra26, doi:10.1126/scitranslmed.3002003 (2011).
621 15 Janne, P. A. *et al.* AZD9291 in EGFR inhibitor-resistant non-small-cell lung cancer. *N Engl J Med*
622 **372**, 1689-1699, doi:10.1056/NEJMoa1411817 (2015).
623 16 Yu, H. A. *et al.* Acquired Resistance of EGFR-Mutant Lung Cancer to a T790M-Specific EGFR
624 Inhibitor: Emergence of a Third Mutation (C797S) in the EGFR Tyrosine Kinase Domain. *JAMA*
625 *Oncol* **1**, 982-984, doi:10.1001/jamaoncol.2015.1066 (2015).
626 17 Fang, W. *et al.* PI3K-AKT-mTOR pathway alterations in advanced NSCLC patients after progression
627 on EGFR-TKI and clinical response to EGFR-TKI plus everolimus combination therapy. *Transl Lung*
628 *Cancer Res* **9**, 1258-1267, doi:10.21037/tlcr-20-141 (2020).

629 18 Chen, H. *et al.* Concomitant genetic alterations are associated with response to EGFR targeted
630 therapy in patients with lung adenocarcinoma. *Transl Lung Cancer Res* **9**, 1225-1234,
631 doi:10.21037/tlcr-20-679 (2020).
632 19 Ludovini, V. *et al.* Phosphoinositide-3-kinase catalytic alpha and KRAS mutations are important
633 predictors of resistance to therapy with epidermal growth factor receptor tyrosine kinase
634 inhibitors in patients with advanced non-small cell lung cancer. *J Thorac Oncol* **6**, 707-715,
635 doi:10.1097/JTO.0b013e31820a3a6b (2011).
636 20 Gini, B., Thomas, N. & Blakely, C. M. Impact of concurrent genomic alterations in epidermal
637 growth factor receptor (EGFR)-mutated lung cancer. *J Thorac Dis* **12**, 2883-2895,
638 doi:10.21037/jtd.2020.03.78 (2020).
639 21 Li, B. *et al.* MiR-21 overexpression is associated with acquired resistance of EGFR-TKI in non-small
640 cell lung cancer. *Lung Cancer* **83**, 146-153, doi:10.1016/j.lungcan.2013.11.003 (2014).
641 22 Zhang, Y. & Wang, J. MicroRNAs are important regulators of drug resistance in colorectal cancer.
642 *Biol Chem* **398**, 929-938, doi:10.1515/hsz-2016-0308 (2017).
643 23 Pal, A. S., Bains, M., Agredo, A. & Kasinski, A. L. Identification of microRNAs that promote erlotinib
644 resistance in non-small cell lung cancer. *Biochem Pharmacol*, 114154,
645 doi:10.1016/j.bcp.2020.114154 (2020).
646 24 Zhang, Y., Li, M. & Hu, C. Exosomal transfer of miR-214 mediates gefitinib resistance in non-small
647 cell lung cancer. *Biochem Biophys Res Commun* **507**, 457-464, doi:10.1016/j.bbrc.2018.11.061
648 (2018).
649 25 Lee, R. C., Feinbaum, R. L. & Ambros, V. The C. elegans heterochronic gene lin-4 encodes small
650 RNAs with antisense complementarity to lin-14. *Cell* **75**, 843-854, doi:10.1016/0092-
651 8674(93)90529-y (1993).
652 26 Reinhart, B. J. *et al.* The 21-nucleotide let-7 RNA regulates developmental timing in
653 Caenorhabditis elegans. *Nature* **403**, 901-906, doi:10.1038/35002607 (2000).
654 27 Lagos-Quintana, M., Rauhut, R., Lendeckel, W. & Tuschl, T. Identification of novel genes coding
655 for small expressed RNAs. *Science* **294**, 853-858, doi:10.1126/science.1064921 (2001).
656 28 Andersen, G. B. & Tost, J. Circulating miRNAs as Biomarker in Cancer. *Recent Results Cancer Res*
657 **215**, 277-298, doi:10.1007/978-3-030-26439-0_15 (2020).
658 29 Khoury, S. & Tran, N. Circulating microRNAs: potential biomarkers for common malignancies.
659 *Biomark Med* **9**, 131-151, doi:10.2217/bmm.14.102 (2015).
660 30 Cazzoli, R. *et al.* microRNAs derived from circulating exosomes as noninvasive biomarkers for
661 screening and diagnosing lung cancer. *J Thorac Oncol* **8**, 1156-1162,
662 doi:10.1097/JTO.0b013e318299ac32 (2013).
663 31 Shen, J. *et al.* Plasma microRNAs as potential biomarkers for non-small-cell lung cancer. *Lab Invest*
664 **91**, 579-587, doi:10.1038/labinvest.2010.194 (2011).
665 32 Moyer, V. A. & Force, U. S. P. S. T. Screening for lung cancer: U.S. Preventive Services Task Force
666 recommendation statement. *Ann Intern Med* **160**, 330-338, doi:10.7326/M13-2771 (2014).
667 33 Pinsky, P. F., Bellinger, C. R. & Miller, D. P., Jr. False-positive screens and lung cancer risk in the
668 National Lung Screening Trial: Implications for shared decision-making. *J Med Screen* **25**, 110-112,
669 doi:10.1177/0969141317727771 (2018).
670 34 Chang, L., Zhou, G., Soufan, O. & Xia, J. miRNet 2.0: network-based visual analytics for miRNA
671 functional analysis and systems biology. *Nucleic Acids Res* **48**, W244-W251,
672 doi:10.1093/nar/gkaa467 (2020).
673 35 Liu, L. *et al.* Inhibition of Wnt/beta-catenin pathway reverses multi-drug resistance and EMT in
674 Oct4(+)/Nanog(+) NSCLC cells. *Biomed Pharmacother* **127**, 110225,
675 doi:10.1016/j.biopha.2020.110225 (2020).

676 36 Stewart, D. J. Wnt signaling pathway in non-small cell lung cancer. *J Natl Cancer Inst* **106**, djt356,
677 doi:10.1093/jnci/djt356 (2014).
678 37 Shinohara, H. *et al.* Regulated Polarization of Tumor-Associated Macrophages by miR-145 via
679 Colorectal Cancer-Derived Extracellular Vesicles. *J Immunol* **199**, 1505-1515,
680 doi:10.4049/jimmunol.1700167 (2017).
681 38 Popena, I. *et al.* Effect of colorectal cancer-derived extracellular vesicles on the
682 immunophenotype and cytokine secretion profile of monocytes and macrophages. *Cell Commun*
683 *Signal* **16**, 17, doi:10.1186/s12964-018-0229-y (2018).
684 39 Whiteside, T. L. Exosomes in Cancer: Another Mechanism of Tumor-Induced Immune
685 Suppression. *Adv Exp Med Biol* **1036**, 81-89, doi:10.1007/978-3-319-67577-0_6 (2017).
686 40 Sharma, S. V., Bell, D. W., Settleman, J. & Haber, D. A. Epidermal growth factor receptor mutations
687 in lung cancer. *Nat Rev Cancer* **7**, 169-181, doi:10.1038/nrc2088 (2007).
688 41 Tetsu, O., Hangauer, M. J., Phuchareon, J., Eisele, D. W. & McCormick, F. Drug Resistance to EGFR
689 Inhibitors in Lung Cancer. *Chemotherapy* **61**, 223-235, doi:10.1159/000443368 (2016).
690 42 Sequist, L. V. *et al.* Phase III study of afatinib or cisplatin plus pemetrexed in patients with
691 metastatic lung adenocarcinoma with EGFR mutations. *J Clin Oncol* **31**, 3327-3334,
692 doi:10.1200/JCO.2012.44.2806 (2013).
693 43 Maemondo, M. *et al.* Gefitinib or chemotherapy for non-small-cell lung cancer with mutated
694 EGFR. *N Engl J Med* **362**, 2380-2388, doi:10.1056/NEJMoa0909530 (2010).
695 44 Mitsudomi, T. *et al.* Gefitinib versus cisplatin plus docetaxel in patients with non-small-cell lung
696 cancer harbouring mutations of the epidermal growth factor receptor (WJTOG3405): an open
697 label, randomised phase 3 trial. *Lancet Oncol* **11**, 121-128, doi:10.1016/S1470-2045(09)70364-X
698 (2010).
699 45 Pao, W. *et al.* Acquired resistance of lung adenocarcinomas to gefitinib or erlotinib is associated
700 with a second mutation in the EGFR kinase domain. *PLoS Med* **2**, e73,
701 doi:10.1371/journal.pmed.0020073 (2005).
702 46 Ramalingam, S. S. *et al.* Osimertinib As First-Line Treatment of EGFR Mutation-Positive Advanced
703 Non-Small-Cell Lung Cancer. *J Clin Oncol* **36**, 841-849, doi:10.1200/JCO.2017.74.7576 (2018).
704 47 Lin, C. C. *et al.* Outcomes in patients with non-small-cell lung cancer and acquired Thr790Met
705 mutation treated with osimertinib: a genomic study. *Lancet Respir Med* **6**, 107-116,
706 doi:10.1016/S2213-2600(17)30480-0 (2018).
707 48 Piotrowska, Z. & Sequist, L. V. Epidermal Growth Factor Receptor-Mutant Lung Cancer: New
708 Drugs, New Resistance Mechanisms, and Future Treatment Options. *Cancer J* **21**, 371-377,
709 doi:10.1097/PPO.0000000000000147 (2015).
710 49 Jacobsen, K. *et al.* Convergent Akt activation drives acquired EGFR inhibitor resistance in lung
711 cancer. *Nat Commun* **8**, 410, doi:10.1038/s41467-017-00450-6 (2017).
712 50 Priglinger, E. *et al.* SVF-derived extracellular vesicles carry characteristic miRNAs in lipedema. *Sci*
713 *Rep* **10**, 7211, doi:10.1038/s41598-020-64215-w (2020).
714 51 Rames, M., Yu, Y. & Ren, G. Optimized negative staining: a high-throughput protocol for examining
715 small and asymmetric protein structure by electron microscopy. *J Vis Exp*, e51087,
716 doi:10.3791/51087 (2014).
717 52 Kocijan, R. *et al.* MicroRNA levels in bone and blood change during bisphosphonate and
718 teriparatide therapy in an animal model of postmenopausal osteoporosis. *Bone* **131**, 115104,
719 doi:10.1016/j.bone.2019.115104 (2020).
720 53 Shore, S. *et al.* Small RNA Library Preparation Method for Next-Generation Sequencing Using
721 Chemical Modifications to Prevent Adapter Dimer Formation. *PLoS One* **11**, e0167009,
722 doi:10.1371/journal.pone.0167009 (2016).

723

Table I (Study participants)

Sample ID	Age (yrs, as of 2019)	Gender	Smoking History (pack - year)	Group	Lung-RAD Score		Death Cancer Related
					INITIAL	LATEST	
82	62	M	40	A	2	4A	None
83	64	F	40	A	2	2	None
84	62	F	45	A	2	2	None
85	62	F	30	A	2	2	None
88	45	F	80	A	2	2	None
91	51	F	40	A	2	2	None
96	58	F	45	A	2	2	None
98	56	F	45	A	2	2	None
99	60	M	35	A	2	2	None
100	61	F	30	A	2	4A	None
102	53	F	40	A	2	2	None
104	58	M	50	A	2	2	None
105	53	F	80	A	2	2	None
106	48	M	45	A	2	2	None
111	57	F	60	A	2	2	None
114	61	M	30	A	2	3	None
120	63	F	40	A	2	4A	None
121	57	F	90	A	2	3	None
123	50	F	40	A	2	2	None
124	61	M	50	A	2	2	None
8	50	F	100	B	4	4B	None
12	50	F	55	B	4	4X	None
15	56	F	45	B	4	4B	None
16	42	F	40	B	4	4B	None
30	49	F	55	B	4	4A	Yes
40	55	M	45	B*	4	4B	None
52	44	F	50	B	4	4B	None
53	58	M	27	B	4	4B	None
70	45	M	50	B	4	4X	None
92	61	M	40	B*	4	4A	None
115	51	F	40	B	4	4B	None
135	50	M	25	B*	4	4B/4X	None
138	49	F	100	B	4	4X	Yes
139	52	F	40	B*	4	4A	None
149	57	M	40	B*	4	4B	None
152	49	F	25	B	4	4B	None
159	60	M	60	B	4	4B	None
170	53	F	40	B	4	4B	None
171	55	M	80	B*	4	2	None
183	56	F	40	B	4	4X	None

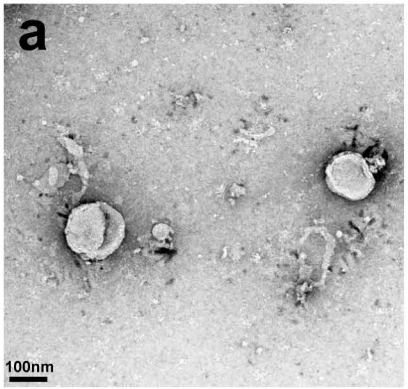
a
100nm

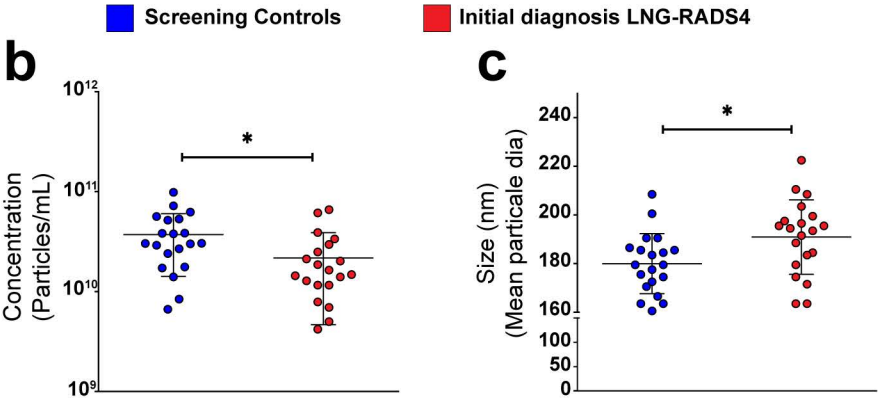
Screening Controls
Initial diagnosis LNG-RADS4
b
Concentration (Particles/mL)
10^{12}
10^{11}
10^{10}
10^{9}
*
c
Size (nm) (Mean particale dia)
240
220
200
180
160
100
50
0
*

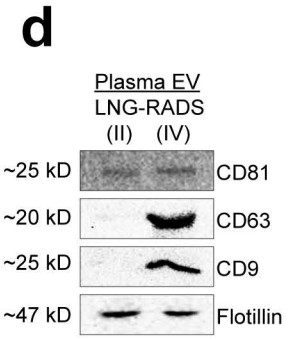
d
Plasma EV
LNG-RADS
(II) (IV)
~25 kD CD81
~20 kD CD63
~25 kD CD9
~47 kD Flotillin

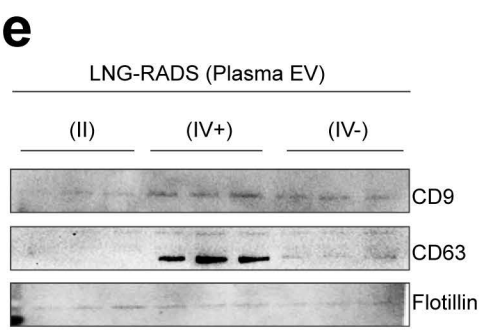
e
LNG-RADS (Plasma EV)
(II)
(IV+)
(IV-)
CD9
CD63
Flotillin

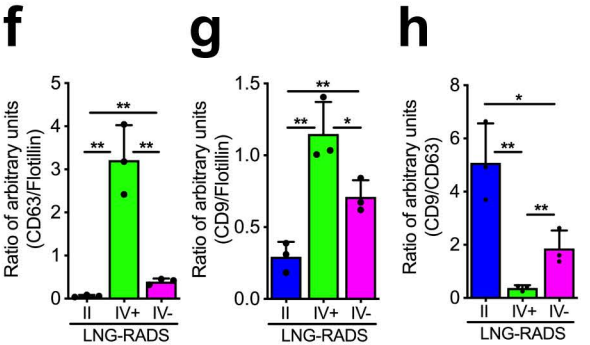
f
Ratio of arbitrary units (CD63/Flotillin)
g
Ratio of arbitrary units (CD9/Flotillin)
h
Ratio of arbitrary units (CD9/CD63)
II
IV+
IV-
LNG-RADS
**
*

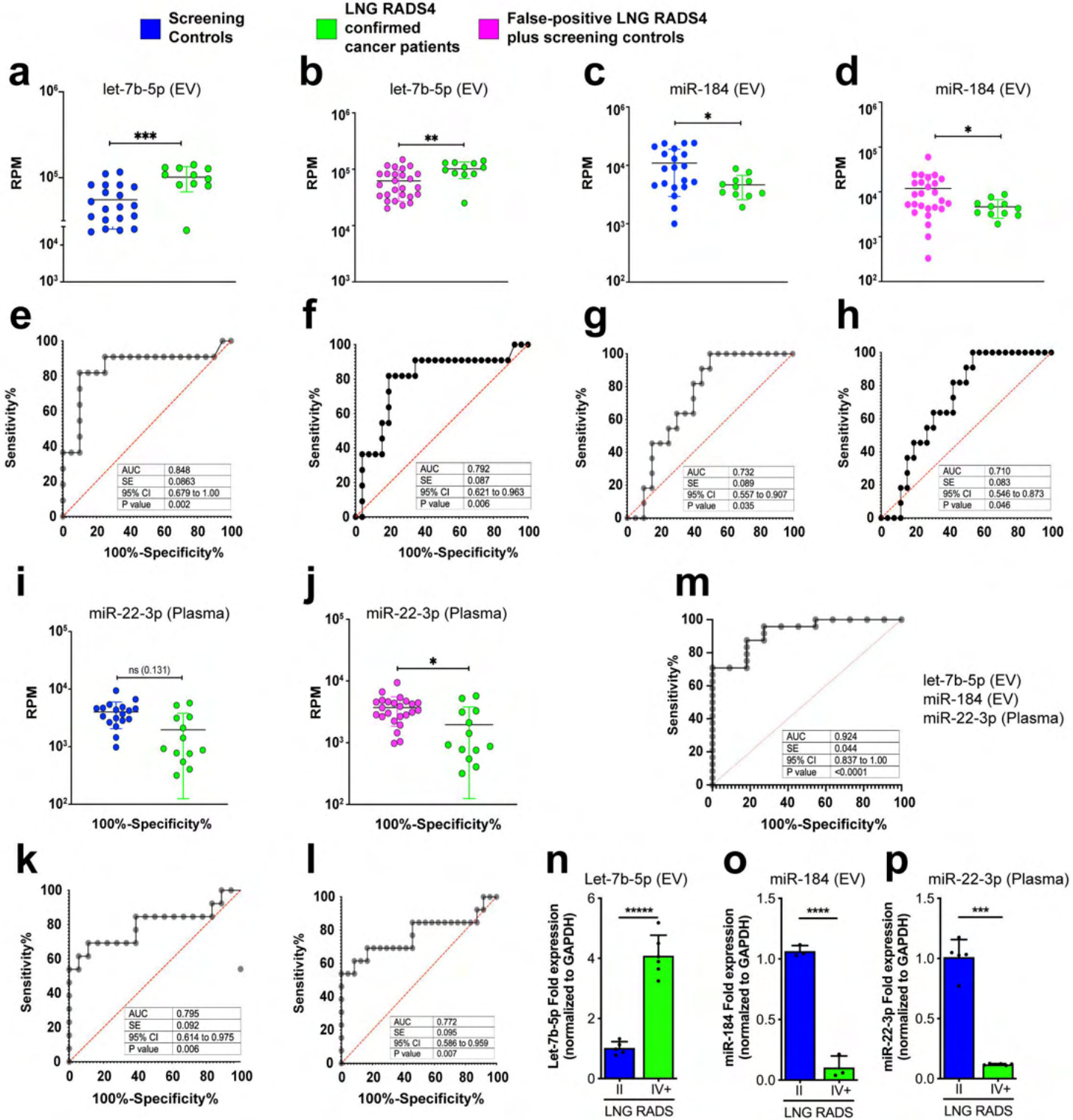
Screening Controls
LNG RADS4 confirmed cancer patients
False-positive LNG RADS4 plus screening controls
a
let-7b-5p (EV)
RPM
***
b
let-7b-5p (EV)
RPM
**
c
miR-184 (EV)
RPM
*
d
miR-184 (EV)
RPM
*
e
Sensitivity%
100%-Specificity%
AUC 0.848
SE 0.0863
95% CI 0.679 to 1.00
P value 0.002
f
Sensitivity%
100%-Specificity%
AUC 0.792
SE 0.087
95% CI 0.621 to 0.963
P value 0.006
g
Sensitivity%
AUC 0.732
SE 0.089
95% CI 0.557 to 0.907
P value 0.035
h
Sensitivity%
AUC 0.710
SE 0.083
95% CI 0.546 to 0.873
P value 0.046
i
miR-22-3p (Plasma)
RPM
ns (0.131)
100%-Specificity%
j
miR-22-3p (Plasma)
RPM
*
100%-Specificity%
m
Sensitivity%
100%-Specificity%
let-7b-5p (EV)
miR-184 (EV)
miR-22-3p (Plasma)
AUC 0.924
SE 0.044
95% CI 0.837 to 1.00
P value <0.0001
k
Sensitivity%
100%-Specificity%
AUC 0.795
SE 0.092
95% CI 0.614 to 0.975
P value 0.006
l
Sensitivity%
100%-Specificity%
AUC 0.772
SE 0.095
95% CI 0.586 to 0.959
P value 0.007
n
Let-7b-5p (EV)
Let-7b-5p Fold expression (normalized to GAPDH)
*****
II
IV+
LNG RADS
o
miR-184 (EV)
miR-184 Fold expression (normalized to GAPDH)
****
II
IV+
LNG RADS
p
miR-22-3p (Plasma)
miR-22-3p Fold expression (normalized to GAPDH)
***
II
IV+
LNG RADS

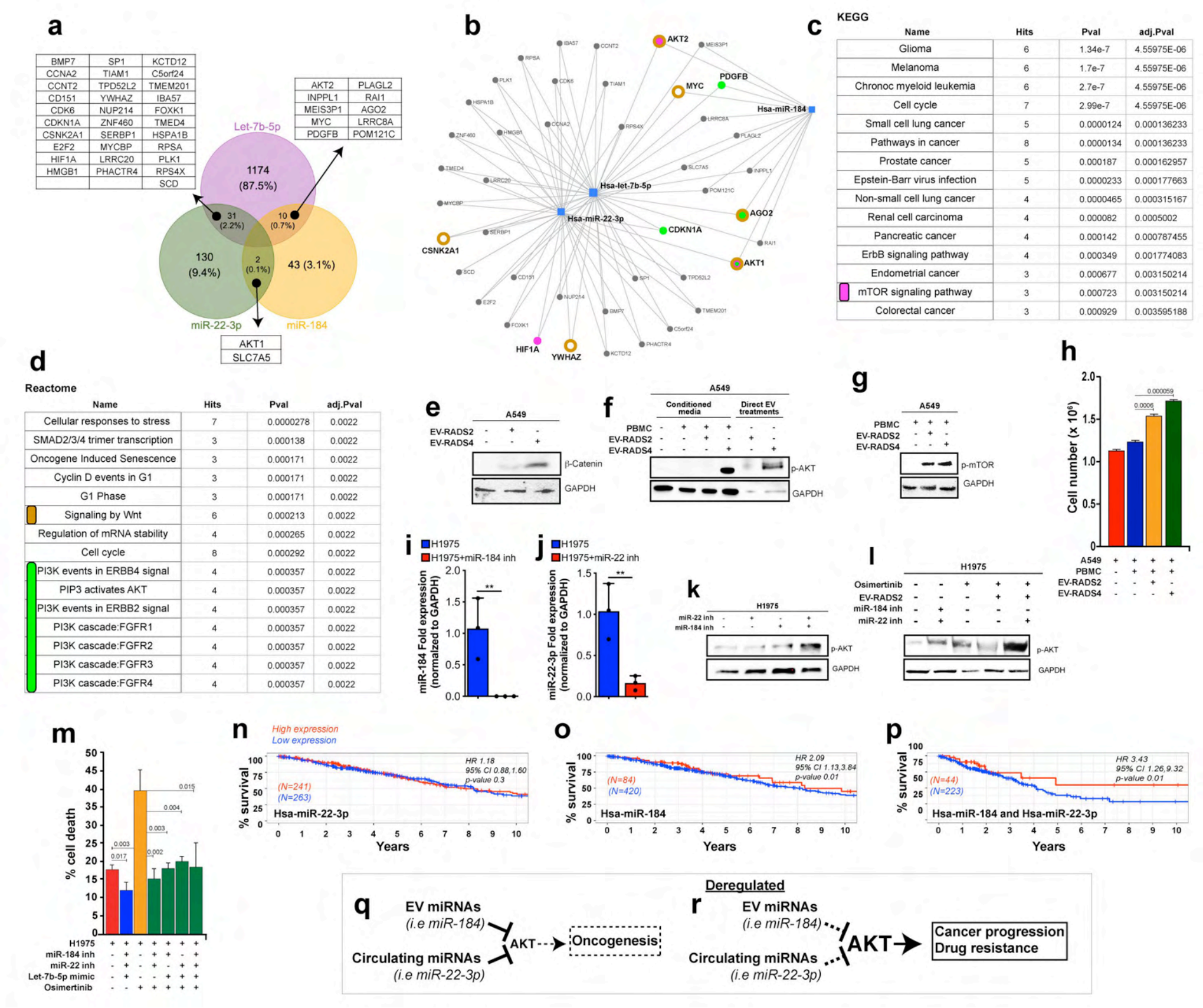

BMP7	SP1	KCTD12
CCNA2	TIAM1	C5orf24
CCNT2	TPD52L2	TMEM201
CD151	YWHAZ	IBA57
CDK6	NUP214	FOXK1
CDKN1A	ZNF460	TMED4
CSNK2A1	SERBP1	HSPA1B
E2F2	MYCBP	RPSA
HIF1A	LRRC20	PLK1
HMGB1	PHACTR4	RPS4X
		SCD

AKT2	PLAGL2
INPPL1	RAI1
MEIS3P1	AGO2
MYC	LRRC8A
PDGFB	POM121C

Name	Hits	Pval	adj.Pval
Glioma	6	1.34e-7	4.55975E-06
Melanoma	6	1.7e-7	4.55975E-06
Chronoc myeloid leukemia	6	2.7e-7	4.55975E-06
Cell cycle	7	2.99e-7	4.55975E-06
Small cell lung cancer	5	0.0000124	0.000136233
Pathways in cancer	8	0.0000134	0.000136233
Prostate cancer	5	0.000187	0.000162957
Epstein-Barr virus infection	5	0.0000233	0.000177663
Non-small cell lung cancer	4	0.0000465	0.000315167
Renal cell carcinoma	4	0.000082	0.0005002
Pancreatic cancer	4	0.000142	0.000787455
ErbB signaling pathway	4	0.000349	0.001774083
Endometrial cancer	3	0.000677	0.003150214
mTOR signaling pathway	3	0.000723	0.003150214
Colorectal cancer	3	0.000929	0.003595188

Name	Hits	Pval	adj.Pval
Cellular responses to stress	7	0.0000278	0.0022
SMAD2/3/4 trimer transcription	3	0.000138	0.0022
Oncogene Induced Senescence	3	0.000171	0.0022
Cyclin D events in G1	3	0.000171	0.0022
G1 Phase	3	0.000171	0.0022
Signaling by Wnt	6	0.000213	0.0022
Regulation of mRNA stability	4	0.000265	0.0022
Cell cycle	8	0.000292	0.0022
PI3K events in ERBB4 signal	4	0.000357	0.0022
PIP3 activates AKT	4	0.000357	0.0022
PI3K events in ERBB2 signal	4	0.000357	0.0022
PI3K cascade:FGFR1	4	0.000357	0.0022
PI3K cascade:FGFR2	4	0.000357	0.0022
PI3K cascade:FGFR3	4	0.000357	0.0022
PI3K cascade:FGFR4	4	0.000357	0.0022